Geophysical Research Letters

RESEARCH LETTER
10.1029/2019GL085933

Ion-Scale Flux Rope Observed inside a Hot Flow Anomaly

Shi-Chen Bai[1,2], Quanqi Shi[1], Terry Z. Liu[3,4,5], Hui Zhang[5], Chao Yue[2,6], Wei-Jie Sun[7], Anmin Tian[1], Alexander W. Degeling[1], Jacob Bortnik[2], I. Jonathan Rae[8], and Mengmeng Wang[1]

[1]Shandong Provincial Key Laboratory of Optical Astronomy and Solar-Terrestrial Environment, School of Space Science and Physics, Institute of Space Sciences, Shandong University, Weihai, China, [2]Department of Atmospheric and Oceanic Sciences, University of California, Los Angeles, CA, USA, [3]University Corporation for Atmospheric Research, Boulder, CO, USA, [4]Department of Earth, Planetary, and Space Sciences, University of California, Los Angeles, CA, USA, [5]Geophysical Institute, University of Alaska Fairbanks, Fairbanks, AK, USA, [6]Institute of Space Physics and Applied Technology, Peking University, Beijing, China, [7]Department of Climate and Space Sciences and Engineering, University of Michigan, Ann Arbor, MI, USA, [8]Mullard Space Science Laboratory, Space and Climate Physics, University College London, UK

Key Points:

- An ion-scale flux rope with 6.1–7.5 ion inertial length is observed at the trailing edge of a hot flow anomaly
- Solar wind ions were decelerated inside the flux rope, and the kinetic energy of solar wind ions was likely converted to the magnetic energy
- The flux rope is close to a one-dimensional structure and expands due to the strong magnetic pressure gradient force

Correspondence to:
Q. Shi,
sqq@pku.edu.cn

Citation:
Bai, S.-C., Shi, Q., Liu, T. Z., Zhang, H., Yue, C., Sun, W.-J., et al. (2020). Ion-scale flux rope observed inside a hot flow anomaly. *Geophysical Research Letters*, *47*, e2019GL085933. https://doi.org/10.1029/2019GL085933

Received 23 OCT 2019
Accepted 1 FEB 2020
Accepted article online 10 FEB 2020

Abstract We report an earthward moving ion-scale flux rope embedded within the trailing edge of a hot flow anomaly (HFA) observed by the Magnetospheric Multiscale satellite constellation on 17 December 2016 upstream of Earth's quasi-parallel bow shock. The driver of the HFA, a tangential discontinuity, was observed by the Wind spacecraft without flux rope signatures around it in the solar wind. This suggests that the earthward moving flux rope was generated inside the HFA. This ion-scale flux rope is not a force free structure and expands due to a strong magnetic pressure gradient force. Solar wind ions are decelerated inside the flux rope by the static electric field likely caused by the charge separation of solar wind particles. Our observations imply that magnetic reconnection may have occurred inside the HFA. Reconnection and flux ropes may play a role in particle acceleration/heating inside foreshock transients.

Plain Language Summary Energetic particles are often observed inside the foreshock transients or in the foreshock region. The acceleration mechanisms of these energetic particles remain an open question. Possible candidates responsible for the acceleration have been put forward, such as Fermi acceleration, electron firehose, and lower hybrid drift instabilities and magnetic reconnection. However, to date, magnetic reconnection is only found in hybrid simulations during the generation of foreshock transients, but never reported by in situ observations. In this paper, we report an ion-scale flux rope observed at the trailing edge of a hot flow anomaly, which could be generated during the magnetic reconnection. Our observations indicate that reconnection could occur locally within foreshock transients and contribute to their particle acceleration.

1. Introduction

Hot flow anomalies (HFAs) are frequently observed near Earth's bow shock, which are characterized by a superheated, tenuous, low-field-strength core region (Schwartz et al., 1985; Schwartz et al., 2000; Zhang et al., 2010; Chu et al., 2017; Wang et al., 2013a, 2013b, 2013c; Zhao et al., 2015, 2017). The streaming energy of the solar wind ion beams and reflected ion beams is converted into the thermal energy inside HFAs, which leads to the expansion of HFAs. Because of the expansion, a strong deflection of the plasma velocity is exhibited within the structure, and the magnetic field and plasma compression regions or secondary shock is presented on one or both sides of the core (Thomsen et al., 1988; Omidi & Sibeck, 2007; Zhang et al., 2010).

Energetic particles up to hundreds of keV have been observed inside the cores of foreshock transients and most of foreshock transients can accelerate/heat particles (Wilson et al., 2016; Liu, Angelopoulos, Hietala, et al., 2017), which raises the question of how particles are accelerated and heated inside the structure. The Fermi acceleration through particle bouncing between the bow shock and the earthward moving boundary of foreshock transients is one possible candidate, which has been carefully investigated recently (Liu, Lu, et al. 2017; Liu et al., 2018; Turner et al., 2018). Recent observations also showed that the betatron acceleration can explain hundreds of keV electrons inside foreshock transients (Liu et al., 2019). The electron firehose and lower hybrid drift instabilities are also possible candidates for the isotropization and heating processes within HFAs (Eastwood et al., 2008; Zhang et al., 2010). Magnetic reconnection during the

development of HFA might be another possible mechanism for the particle acceleration inside HFAs (Lin, 1997). A particle-in-cell simulation shows that suprathermal electrons were accelerated by the magnetic islands generated by magnetic reconnection in the quasi-perpendicular shock (Matsumoto et al., 2015). Reconnection is also shown to occur in the quasi-parallel shock transition region through the Weibel instability (Gingell et al., 2017). If magnetic reconnection occurs inside foreshock transients, Fermi acceleration during the coalescence of magnetic islands could be another potential mechanism.

Recently, features of current sheet structures consistent with magnetic reconnection were found in the transition region of a quasi-parallel shock (Gingell et al., 2019; Hamrin et al., 2019) and quasi-perpendicular shock (Wang et al., 2019) with Magnetospheric Multiscale (MMS) high cadence plasma measurements. Signatures of magnetic reconnection such as small-scale flux ropes, which formed due to the tearing mode instability (Daughton et al., 2006; Drake, Swisdak, & Che, et al., 2006) or electron Kelvin-Helmholtz instability (Fermo et al., 2012) during the reconnection, might be found inside foreshock transients. To date, only a magnetic flux rope event in the magnetosheath part of an HFA has been reported (Hasegawa et al., 2012), which probably originates from magnetic reconnection in the magnetosheath part of the HFA. However, there is no clear observation of flux ropes formed locally inside foreshock transients.

In this study, we report an ion-scale flux rope observed at the trailing edge of an HFA in the ion foreshock, which is expanding and moving earthward with the HFA. The paper is organized as follows. In section 2.1, we introduce the data used in this study. In section 2.2, an overview of the HFA observed by MMS is given, in which the ion-scale flux rope is encountered. The solar wind condition observed by ACE and Wind is also provided in this section. Detailed analysis of the flux rope embedded in the HFA is presented in section 2.3. The expansion of the flux rope is investigated in section 2.4. Section 3 briefly discusses the mechanism of the expansion of the ion-scale flux rope and the energy transfer around the flux rope.

2. Observations

2.1. Data

In this paper, the solar wind magnetic field is measured by the magnetometer onboard the Wind satellite (Lepping et al., 1995) and ACE satellite (Smith et al., 1998). The foreshock observation comes from the fluxgate magnetometer (Russell et al., 2016), the fast plasma investigation (FPI; Pollock et al., 2016), and the electric field double probes (EDP; Lindqvist et al., 2016; Ergun et al., 2014) onboard the MMS satellite constellation (Burch et al., 2016).

2.2. MMS Observation of an HFA

The time scale of the observed HFA is only 16 s, extending from 12:55:12 UT to 12:55:28 UT, located upstream of a quasi-parallel shock ($\theta_{Bn} = 43°$, determined by using the bow shock model (Slavin & Holzer, 1981) shown in the black dashed box in Figure 1. The magnitude of the magnetic field and the electron density increased at both edges and decreased in the core region of the HFA (Figures 1(a) and 1(b)), which is caused by the expansion of the HFA (Thomsen et al., 1988; Omidi & Sibeck, 2007). The electron temperature increases continuously inside the HFA (Figure 1(c)); this might be related to the earthward motion of the HFA and the Fermi acceleration of electrons (Liu, Lu, et al., 2017). The electron velocity decreases inside the HFA (Figure 1(d)). Energetic foreshock ions (Figure 1(e)) get thermalized inside the HFA, which provides the energy for the expansion of the HFA (Onsager et al., 1990). All of these are typical observational features of HFAs. The HFA was expanding and moving toward the bow shock based on timing analysis (Schwartz, 1998). The velocities of the leading and trailing edges of the HFA are $165.8 \pm 7.6 \times [-0.96, 0.01, 0.24]$ km/s and $91.9 \pm 3.6 \times [-0.90, -0.29\text{-}0.31]$ km/s in GSM coordinates, respectively.

The prevailing solar wind parameters, observed by ACE and Wind, are shifted to the MMS location (Figures 1(g) and 1(h)). Because of the large disturbance in the magnetic field, the comparison of cone/clock angle between MMS and Wind/ACE was not used when MMS was in the foreshock region and not shown in Figures 1(i)–1(j). Using only the time interval when MMS was in the solar wind before and after the event, the comparison of the cone angle and clock angle of the interplanetary magnetic field (IMF) observed by ACE, Wind, and MMS are shown in Figures 1(i) and 1(j) and the lag time between ACE/Wind and MMS is determined by the highest correlation coefficient of the cone angle ($r > 0.9$). Within this time interval, there is only one possible discontinuity observed by Wind at ~12:55:04 UT (blue

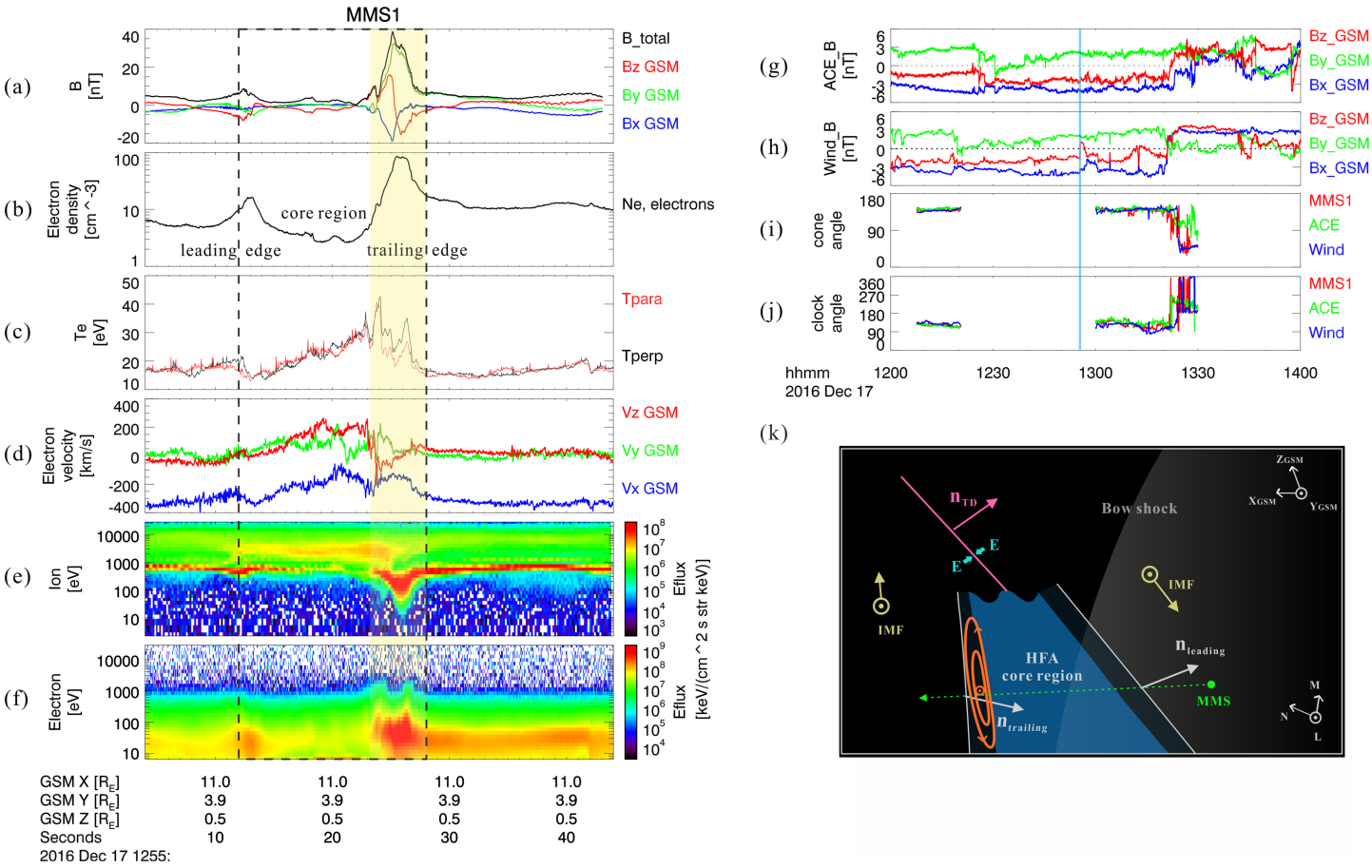

Figure 1. An overview plot of MMS1 observation of the flux rope inside the HFA. The blue/green/red line for *X*/*Y*/*Z* component in GSM coordinate. From top to bottom: A magnetic field; b electron number density; c electron parallel (red line) and perpendicular (black line) temperature; d electron velocity; e omnidirectional ion energy flux; f omnidirectional electron energy flux; g magnetic field observed by ACE and shifted to the MMS location; h magnetic field observed by wind and shifted to the MMS location; i IMF cone angle observed by ACE, wind, and MMS1; j IMF clock angle of IMF observed by ACE, wind, and MMS1; k illustration of the HFA and the relative trajectory of MMS. To better illustrate the flux rope, HFA, and bow shock, *X* and *Z* are not perpendicular to each other. *M* and *N* are not perpendicular to each other too. The normal directions of both edges are not perpendicular to the edges. The normal direction of the TD is not perpendicular to the TD in panel (k). The HFA is marked by the black dashed box, and the flux rope is marked by the yellow shaded region. The time interval of Figures 1(a)–1(f) is marked by the blue shaded region in Figures 1(g)–1(j).

shaded region; only a weak variation is observed by ACE) that might trigger the generation of the HFA. It is a tangential discontinuity (TD) identified by a near-zero normal component and a discontinuity in the tangential component of the magnetic field around it. The normal of the TD is [−0.543, −0.830, 0.122] in GSM coordinates determined by the minimum variance analysis (Sonnerup & Cahill, 1967; MVAB), and a similar normal is obtained through the cross product method (Schwartz, 1998) at Wind. The propagation of the TD is consistent with the time delay from Wind to MMS. The motional electric field ($E = -V \times B$) points toward the TD on both sides, consistent with the preferred condition for the HFA generation (Thomsen et al., 1993). During the entire time interval around the discontinuity, no flux rope signature, such as the unipolar component and bipolar component of magnetic field, is shown. A schematic illustration of the TD, the HFA, and the relative trajectory of MMS is shown in Figure 1(k).

2.3. Ion-Scale Flux Rope

At the trailing edge of the HFA (Figures 1–3 shaded region; 12:55:23 UT to 12:55:28 UT), the magnetic field strength and the electron density enhancement at the trailing edge are very significant. The electron density increased from 11.35 cm^{-3} in the solar wind to 80.98 cm^{-3} at the trailing edge of the HFA and the magnetic field strength also increased from 4.5 nT in the solar wind to 34.0 nT at the trailing edge of the HFA with a compression ratio much larger than 4. This means that it is not a typical compressional boundary. The

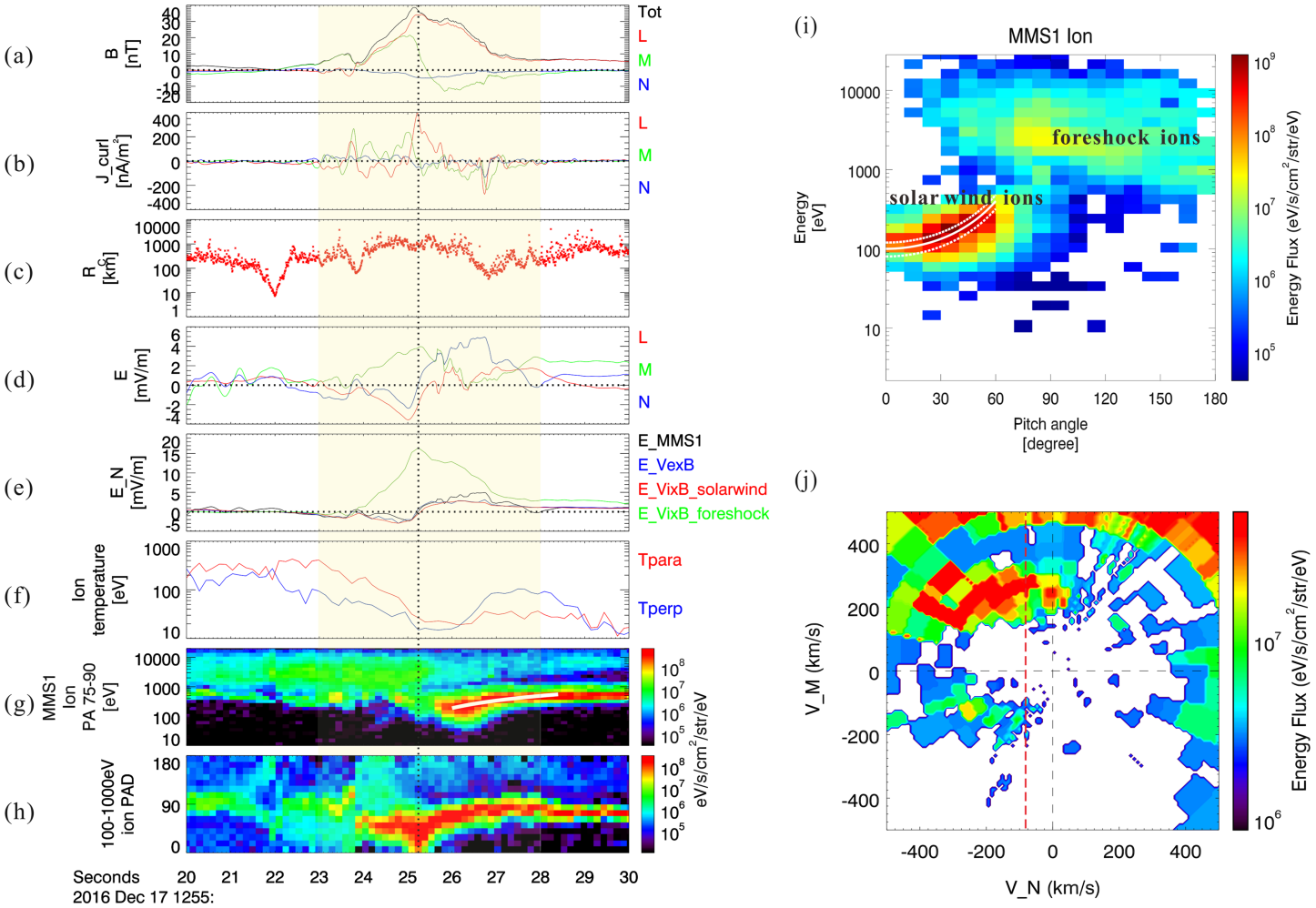

Figure 2. MMS observation of the flux rope in *L-M-N* coordinate from 12:55:23 to 12:55:28 UT marked by the yellow shade region. The blue/green/red line represents the *L*/*M*/*N* component. From top to bottom: A magnetic field; b current density; c the radius of magnetic curvature Rc; d electric field; e *N* component of the electric field with the black from the MMS1 measurements, red from the foreshock ion motion, green from the solar wind ion motion, and blue from the electron motion; f perpendicular and parallel temperature of the solar wind ions; g perpendicular ion energy flux; h 100–1,000 eV ion pitch angle distribution; i the ion distribution (eV/s/cm^2/str/eV) displays as a function of energy and pitch angle at 12:55:25.24 UT (vertical dashed line in Figures 2(a)–2(g)); j the ion distribution (eV/s/cm^2/str/eV) in the *M*-*N* plane at 12:55:25.24 UT. The white solid line in Figure 2(f) is the solar wind energy decrease as 1.7 mV/m · 133.56 km in the de Hoffmann teller frame (V_{HT} = 232.5 × [−0.96, 0.28,0.07] km/s) and transformed it back to the spacecraft frame. The curved lines in the Figure 2(h), given by $\theta = \cos^{-1}[(E_{//}/E)^{1/2}]$, show the contour line of parallel energy $E_{//}$=80 eV (dashed line), 100 eV (solid line), and 120 eV (dashed line). The red dashed line is the velocity (V_N = −89.04 km/s) of the trailing edge of the HFA base on the timing analysis.

bipolar B_z and unipolar B_y suggest that it could be a small-scale flux rope. Using the timing analysis (Schwartz, 1998), the velocities of the leading and trailing edges of the flux rope are 113.5 ± 5.9 × [−0.84, −0.32, −0.43] km/s and 91.93 ± 3.6 × [−0.90, −0.29, −0.31] km/s in GSM coordinate, respectively. This suggests that the flux rope is expanding at ~20 km/s toward the sun in the solar wind reference frame. The spatial scale of the flux rope is 6.10–7.51 ion inertial lengths. The ion inertial length here is 75.5 km determined by the ion density in the solar wind (12:55:30–12:55:40 UT). The expansion of the flux rope will be carefully investigated in the next section.

To better investigate this case, we use the *L-M-N* coordinate system, which is determined by MVAB (Sonnerup & Cahill, 1967). We found that *L* ~[−0.18, 0.98, −0.07], *M* ~[−0.46, −0.02, 0.88], *N* ~[0.86, 0.19, 0.45] are the maximum, intermediate, and minimum variation directions in GSM coordinates, respectively. The core field of the flux rope is in the *L* direction, and the bipolar signature is shown in the *M* direction. B_N is negative and decreased inside the flux rope. Field-aligned current, which is calculated using the culometer

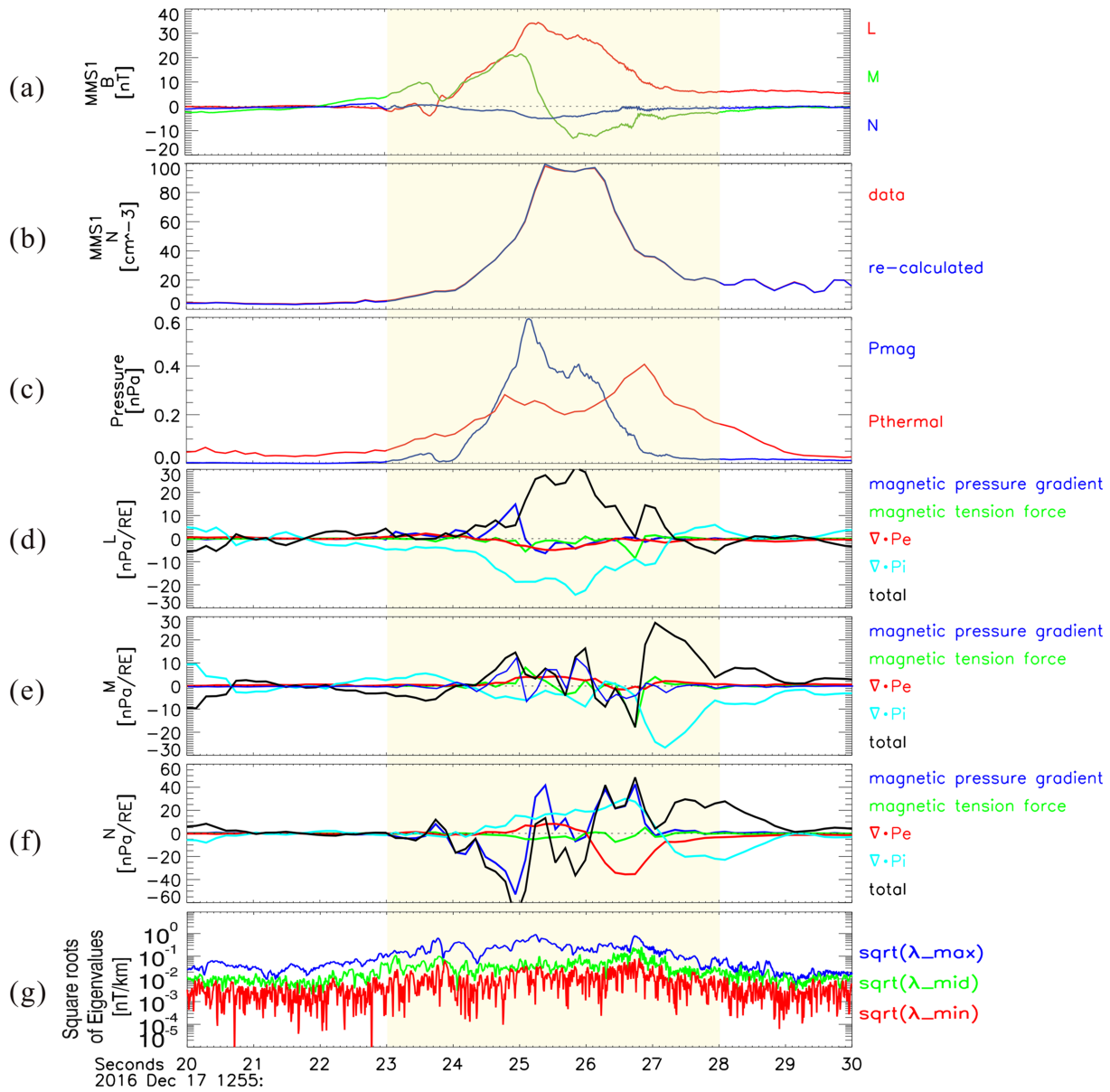

Figure 3. A magnetic field in *L-M-N* coordinates; b ion density from MMS1 FPI data shown in red and from the recalculated MMS1 FPI data shown in blue; c magnetic pressure shown in blue and thermal pressure shown in red; d *L* component of the force analysis; e *M* component of the force analysis; f *N* component of the force analysis with the black being the summation of different force contribution, the blue being the magnetic pressure gradient force, the green being the magnetic tension force, the cyan being the ion pressure gradient force, and red being the electron pressure gradient force; g eigenvalues resulted from MDD, $\sqrt{\lambda_{\max}}$ is in blue, $\sqrt{\lambda_{\mathrm{mid}}}$ in green, and $\sqrt{\lambda_{\min}}$ in red; the flux rope is marked by the yellow shaded region.

technique (Dunlop et al., 1988, 2002), was observed at the center of the flux rope (Figure 2(b)). Due to the presence of helical structure inside the flux rope, the local radius of curvature of the magnetic field lines increases from 300 to 1,000 km inside the flux rope (Figure 2(c)), which is obtained by magnetic field rotation analysis (Shen et al., 2007). The observational features of the magnetic field, current density, and radius of curvature of the magnetic field lines listed above are consistent with the previous work on flux ropes (e.g., Russell & Elphic, 1979; Slavin et al., 2003; Shen et al., 2007; Zong et al., 2004; Sun et al., 2019).

The electric field is shown in Figure 2(d), and we focus on the component in the normal direction. Two ion populations were observed inside the flux rope, one comes from the solar wind from 10 to 1,000 eV and the other from the foreshock ions from 1 to 3 keV (see Figure 1(e)). The $\mathbf{V} \times \mathbf{B}$ of these two ion populations are

quite different. The $\mathbf{V_{i\_solarwind}} \times \mathbf{B}$ agrees well with the $\mathbf{V_e} \times \mathbf{B}$. For foreshock ions, on the other hand, the $\mathbf{V_{i\_foreshock}} \times \mathbf{B}$ does not match the $\mathbf{V_e} \times \mathbf{B}$ at all. There is also disagreement between the $\mathbf{V_e} \times \mathbf{B}$ and the electric field measured by EDP from 12:55:26 to 12:55:27.5 UT. One possible reason is that when the solar wind penetrates the flux rope, the gyroradii difference between the solar wind ions and electrons generates the electrostatic field in normal direction, which could decelerate the solar wind ions. Considering the velocity of the trailing edge of the HFA, the spatial scale of this disagreement electric field is 133.56 km, which is close to the gyroradii difference between the solar wind ions and electrons (142.03 km for 1-keV solar wind particles). To further confirm this, we calculated this static electric field in $+N$ direction through the disagreement between EDP measurement and $\mathbf{V_e} \times \mathbf{B}$ and compared it with the energy decrease of solar wind ions. Here we used the average value of the disagreement between the $\mathbf{V_e} \times \mathbf{B}$ and the measured electric field from 12:55:26 to 12:55:27.5 UT as the static electric field E = 1.7 mV/m. Then we calculated the solar wind energy decrease as 1.7 mV/m · 133.56 km in the de Hoffmann Teller frame (Sonnerup et al., 1987; $V_{\mathrm{HT}} = 232.5 \times [-0.96, 0.28, 0.07]$ km/s) and transformed it back to the spacecraft frame shown as the white solid lines in Figure 2(g). It matches the energy where the solar wind ion flux peaks very well, confirming the deceleration of solar wind ions by the static electric field at the trailing edge of flux rope. There is no significant change in the Tpara of the solar wind ions around the trailing edge of the flux rope (red in Figure 2(f)). The Tperp (blue in Figure 2f), on the other hand, increases during the deceleration of solar wind ions at the boundary of the flux rope possibly due to the magnetic field strength enhancement. At the peak of the field strength where J_L reaches the peak, however, the perpendicular temperature decreases, and the parallel motion dominates (Figure 2(h)). This is again inconsistent with typical compressional boundaries or shocks, but more consistent with field-aligned particle motion inside flux ropes.

To see it more clearly, Figure 2(i) show the ion distribution at 12:55:25.24 UT (marked by the vertical dashed line) when the field-aligned current peaked. The white dashed and solid lines overlaid in Figure 2(i) represent the ions with the same parallel velocity, suggesting that the solar wind ions are decelerated and thermalized in the perpendicular plane inside the flux rope than in the solar wind. Figure 2(i) shows the ion distribution in the *M*-*N* plane (roughly the plane perpendicular to the magnetic field as B_L dominates), the $E \times B$ motion of the solar wind ions is mainly in the *M* direction, and the thermalization of the solar wind ions is mainly in the *N* direction. The red dashed line in Figure 2(j) is the velocity of trailing edge of the flux rope in the normal direction. Most of the solar wind ions are faster than that speed (Vn).

2.4. Force Analysis inside the Flux Rope

To understand why the structure is expanding, Figure 3 shows the pressure and force analysis inside the flux rope. Because the spatial scale of the flux rope is too small compared to the gyroradii (~710 km) of foreshock ions and the foreshock ion density is much lower than the solar wind ion density, we ignore the pressure and pressure gradient force caused by the foreshock ions inside the flux rope and separate the solar wind ions (10–1,000 eV) from the total ion distribution. However, foreshock ions still contribute to the current and electrostatic field inside the flux rope. Before we analyze each term on the right side of the MHD momentum equation (equation (1)), we test the reliability of our calculation by comparing the sum of the ion density calculated by two ion populations with the MMS measurement (Figure 3(b)), which shows excellent agreement.

As shown in Figure 3(c), the magnetic pressure is enhanced at the center of the flux rope and the thermal pressure reaches the two peaks at two edges of the flux rope. Each term on the right side of the momentum equation shown below is calculated in *L*-*M*-*N* coordinates and displayed in Figures 3(d)–3(f). The pressure gradients are calculated based on the pressure tensor.

In the *L* direction (Figure 3(d)), the ion pressure gradient determines the motion of the flux rope, whereas the other three terms are insignificant inside the flux rope. In the *M* direction, the motion of the flux rope is determined by the magnetic pressure gradient and ion pressure gradient force. The *M* component of the magnetic pressure gradient and magnetic tension force (Figure 3(e)) changes direction during the MMS crossing, indicating that the MMS is crossing the center of the flux rope rather than a pressure pulse driven structure; otherwise, the M component should be unidirectional (Sibeck, 1990; Lockwood, 1991). In the *N* direction (Figure 3(f)), the magnitude of the magnetic pressure gradient force is much larger than the other two terms and determines the expansion of the flux rope. Magnetic tension force in the normal direction is

very weak inside the flux rope, which suggests that the field line might be elongated in the *M* direction rather than circular in the *M-N* plane. Another piece of evidence to support this point is that the dimension of this flux rope is quasi-one-dimensional (1-D) rather than two-dimensional (2-D) structure as usual, which is determined by the minimum directional derivative method (Shi et al., 2005; Shi et al., 2019). The structure should be 1-D when $\sqrt{\lambda_{max}} \gg \sqrt{\lambda_{mid}}, \sqrt{\lambda_{min}}$ as shown in Figure 3(g). λ_{max}, λ_{mid}, and λ_{min} are three eigenvalues of a symmetrical matrix $L = GG^T = \left(\nabla \overrightarrow{B}\right)\left(\nabla \overrightarrow{B}\right)^T$, which represent the maximum, intermediate, and minimum values of the field directional derivatives, respectively.

3. Summary and Discussion

In this paper, we report a small-scale flux rope with the width of 6.1–7.5 ion inertial lengths at the trailing edge of the HFA in the foreshock for the first time, which is characterized by the bipolar signature of the B_M component, a strong core field, and field-aligned current. Inside the flux rope, the perpendicular temperature decreased, and the *M* components of the magnetic gradient force changes direction several times. Both features further support that it is a flux rope, rather than a typical compressional boundary at the trailing edge of the HFA. A TD was observed in the solar wind, which may leads to the generation of the HFA. However, no flux rope signature was observed in the solar wind around the discontinuity and the flux rope is moving toward the bow shock, indicating that the ion-scale flux rope is locally generated at the trailing edge of the HFA, rather than being generated in the magnetosheath or in the solar wind and propagating to the core region of the HFA.

Solar wind ions are decelerated at the boundary of the flux rope between 12:55:26 and 12:55:28 UT, which is related to the positive static E_N pointing toward the solar wind possibly caused by the charge separation of the solar wind particles. The perpendicular temperature of solar wind ions (10–1,000 eV) increased simultaneously, indicating that solar wind ions at the HFA boundary are strongly diffused in the normal direction, and the kinetic energy of solar wind ions is converted into the thermal energy. Inside the flux rope, however, the parallel ion motion dominates. These parallel motion-dominated solar wind ions could be decelerated by the $-L$ electric field and eventually trapped inside the flux rope, which may lead to the unusual high density observed by MMS. There is no enhancement of the thermal energy inside the flux rope. Instead, the perpendicular temperature decreases although the magnetic field strength continues to increase. The kinetic energy of solar wind ions was probably converted to the magnetic energy with the local $J \cdot E'$ in the flux rope close to $-0.9 nW/m^3$. These features further indicate that the trailing edge of the HFA is not a typical compressional boundary or shock, but a flux rope.

The *M* component of the magnetic pressure gradient and magnetic tension changes directions several times during the flux rope crossing, indicating that the MMS crosses the center of the flux rope. The *N* component of the magnetic tension force is close to zero, indicating that the flux rope is a quasi-1-D structure, which is easier to be observed in the magnetic reconnection with small guide field than quasi-2-D flux rope (Sun et al., 2019). This transient quasi-1-D flux rope is not a force free structure and expanding mainly in the normal direction, which is determined by the magnetic pressure gradient force. Therefore, reconnection might be triggered within the HFA at the early stage during the interaction between the discontinuity and the bow shock, which is consistent with the hybrid simulation (Lin, 1997) and MMS observation (Hamrin et al., 2019). Additionally, this provides another way to generate energetic electrons inside foreshock transients that electrons could be accelerated up to hundreds of keV during the coalescence of ion-scale flux ropes (Drake, Swisdak, & Schoeffler et al., 2006; Matsumoto et al., 2015). However, electrons with hundreds of keV were not observed in this case, which might have not been generated yet or have leaked to the foreshock region like energetic ions (Liu, Angelopoulos, & Hietala, 2017). Our observations of the ion-scale flux rope inside the HFA fills in the blank of in situ observation of reconnection signature inside foreshock transients and might shed light on the particle acceleration in the foreshock region.

Acknowledgments
MMS data are available at MMS Science Data Center (https://lasp.colorado.edu/mms/sdc/). This work was supported by the National Natural Science Foundation of China (Grants 41974189, 41774153, and 41961130382) and the Royal Society NAF\R1\191047], Project Supported by the Specialized Research Fund for State Key Laboratories, International Space Science Institute (ISSI), and the young scholar plan of Shandong University at Weihai (2017WHWLJH08). S.-C. B. is supported by the State Scholarship Fund of Chinese Scholarship Council. I. J. R. is funded in part by STFC Grant ST/N0007722/1 and ST/S000240/1 and Natural Environment Research Council (NERC) Grants NE/P017150/1 and NE/P017185/1. T. Z. L. is supported by the NASA Living With a Star Jack Eddy Postdoctoral Fellowship Program, administered by the Cooperative Programs for the Advancement of Earth System Science (CPAESS). H. Z. is partially supported by NSF AGS-1352669. J. B. is supported by Grant NNX14AI18G from the National Aeronautics and Space Administration (NASA).

References

Burch, J. L., Moore, T. E., Torbert, R. B., & Giles, B. L. (2016). Magnetospheric multiscale overview and science objectives. *Space Sci. Rev.*, *199*(1-4), 5–21. https://doi.org/10.1007/s11214-015-0164-9

Chu, C. S., Zhang, H., Sibeck, D. G., Otto, A., Zong, Q., Omidi, N., et al. (2017). THEMIS satellite observations of hot flow anomalies at Earth's bow shock. *Annales de Geophysique*, *35*(3), 443–451. https://doi.org/10.5194/angeo-35-443-2017

Daughton, W., Scudder, J., & Karimabadi, H. (2006). Fully kinetic simulations of undriven magnetic reconnection with open boundary conditions. *Physics of Plasmas*, *13*(7), 072101. https://doi.org/10.1063/1.2218817

Drake, J. F., Swisdak, M., Che, H., & Shay, M. A. (2006). Electron acceleration from contracting magnetic islands during reconnection. *Nature*, *443*(7111), 553–556. https://doi.org/10.1038/nature05116

Drake, J. F., Swisdak, M., Schoeffler, K. M., Rogers, B. N., & Kobayashi, S. (2006). Formation of secondary islands during magnetic reconnection. *Geophysical Research Letters*, *33*(13), L13105. https://doi.org/10.1029/2006GL025957

Dunlop, M. W., Balogh, A., Glassmeier, K.-H., & Robert, P. (2002). Four-point cluster application of magnetic field analysis tools: The Curlometer. *Journal of Geophysical Research*, *107*(A11), 1384. https://doi.org/10.1029/2001JA005088

Dunlop, M. W., Southwood, D. J., Glassmeier, K.-H., & Neubauer, F. M. (1988). Analysis of multipoint magnetometer data. *Advances in Space Research*, *8*(273), 1988. https://doi.org/10.1016/0273-1177(88)90141-x

Eastwood, J. P., Sibeck, D. G., Angelopoulos, V., Phan, T. D., Bale, S. D., McFadden, J. P., et al. (2008). THEMIS observations of a hot flow anomaly: Solar wind, magnetosheath, and ground-based measurements. *Geophys. Res. Lett.*, *35*(17), L17S03. https://doi.org/10.1029/2008GL033475

Ergun, R. E., Tucker, S., Westfall, J., Goodrich, K. A., Malaspina, D. M., Summers, D., et al. (2014). The axial double probe and fields signal processing for the MMS mission. *Space Sci. Rev.*, *199*(1-4), 167–188. https://doi.org/10.1007/s11214-014-0115-x

Fermo, R. L., Drake, J. F., & Swisdak, M. (2012). Secondary magnetic islands generated by the kelvin-Helmholtz instability in a reconnecting current sheet. *Physical Review Letters*, *108*(25), 255,005. https://doi.org/10.1103/PhysRevLett.108.255005

Gingell, I., Schwartz, S. J., Burgess, D., Johlander, A., Russell, C. T., Burch, J. L., et al. (2017). MMS observations and hybrid simulations of surface ripples at a marginally quasi-parallel shock. *Journal of Geophysical Research: Space Physics*, *122*(11), 11,003–11,017. https://doi.org/10.1002/2017JA024538

Gingell, I., Schwartz, S. J., Eastwood, J. P., Burch, J. L., Ergun, R. E., Fuselier, S., et al. (2019). Observations of magnetic reconnection in the transition region of quasi-parallel shocks. *Geophysical Research Letters*, *46*(3), 1177–1184. https://doi.org/10.1029/2018GL081804

Hamrin, M., Gunell, H., Goncharov, O., De Spiegeleer, A., Fuselier, S., Mukherjee, J., et al. (2019). Can reconnection be triggered as a solar wind directional discontinuity crosses the bow shock?—A case of asymmetric reconnection. Journal of Geophysical Research: Space Physics, 124(11), 8507-8523. https://doi.org/10.1029/2019JA027006

Hasegawa, H., Zhang, H., Lin, Y., Sonnerup, B. U. Ö., Schwartz, S. J., Lavraud, B., & Zong, Q.-G. (2012). Magnetic flux rope formation within a magnetosheath hot flow anomaly. *Journal of Geophysical Research*, *117*(A9), A09214. https://doi.org/10.1029/2012JA017920

Lepping, R. P., Acũna, M. H., Burlaga, L. F., Farrell, W. M., Slavin, J. A., Schatten, K. H., et al. (1995). The WIND magnetic field investigation. *Space Sci. Rev.*, *71*(1-4), 207–229. https://doi.org/10.1007/BF00751330

Lin, Y. (1997). Generation of anomalous flows near the bow shock by its interaction with interplanetary discontinuities. *Journal of Geophysical Research*, *102*(A11), 24,265–24,281. https://doi.org/10.1029/97JA01989

Lindqvist, P.-A., Olsson, G., Torbert, R. B., King, B., Granoff, M., Rau, G. N., et al. (2016). The spin-plane double probe electric field instrument for MMS. *Magnetospheric Multiscale, Space Sci Rev.*, *199*, 137–165. https://doi.org/10.1007/978-94-024-0861-4_6

Liu, T. Z., Angelopoulos, V., & Hietala, H. (2017). Energetic ion leakage from foreshock transient cores. *J. Geophys. Res. Space Physics*, *122*, 7209–7225. https://doi.org/10.1002/2017JA024257

Liu, T. Z., Angelopoulos, V., Hietala, H., & Wilson, L. B. III (2017). Statistical study of particle acceleration in the core of foreshock transients. *J. Geophys. Res. Space Physics*, *122*(7), 7197–7208. https://doi.org/10.1002/2017JA024043

Liu, T. Z., Angelopoulos, V., & Lu, S. (2019). Relativistic electrons generated at Earth's quasi-parallel bow shock. *Science Advances*, *5*(7), eaaw1368. https://doi.org/10.1126/sciadv.aaw1368

Liu, T. Z., Lu, S., Angelopoulos, V., Hietala, H., & Wilson, L. B. III (2017). Fermi acceleration of electrons inside foreshock transient cores. *J. Geophys. Res. Space Physics*, *122*, 9248–9263. https://doi.org/10.1002/2017JA024480

Liu, T. Z., Lu, S., Angelopoulos, V., Lin, Y., & Wang, X. Y. (2018). Ion acceleration inside foreshock transients. *Journal of Geophysical Research: Space Physics*, *123*, 163–178. https://doi.org/10.1002/2017JA024838

Lockwood, M. (1991). Flux transfer events at the dayside magnetopause: Transient reconnection or magnetosheath dynamic pressure pulses? *Journal of Geophysical Research*, *96*(A4), 5497–5509. https://doi.org/10.1029/90JA02389

Matsumoto, Y., Amano, T., Kato, T. N., & Hoshino, M. (2015). Stochastic electron acceleration during spontaneous turbulent reconnection in a strong shock wave. *Science*, *347*(6225), 974–978. https://doi.org/10.1126/science.1260168

Omidi, N., & Sibeck, D. G. (2007). Formation of hot flow anomalies and solitary shocks. *Journal of Geophysical Research*, *112*(A1), A01203. https://doi.org/10.1029/2006JA011663

Onsager, T. G., Thomsen, M. F., Gosling, J. T., & Bame, S. J. (1990). Observational test of a hot flow anomaly formation mechanism. *Journal of Geophysical Research*, *95*(A8), 11,967–11,974. https://doi.org/10.1029/JA095iA08p11967

Pollock, C., Moore, T., Jacques, A., Burch, J., Gliese, U., Saito, Y., et al. (2016). Fast plasma investigation for magnetospheric multiscale. *Space Sci. Rev.*, *199*(1-4), 331–406. https://doi.org/10.1007/s11214-016-0245-4

Russell, C. T., Anderson, B. J., Baumjohann, W., Bromund, K. R., Dearborn, D., Fischer, D., et al. (2016). The magnetospheric multiscale magnetometers. *Space Sci. Rev.*, *199*(1-4), 189–256. https://doi.org/10.1007/s11214-014-0057-3

Russell, C. T., & Elphic, R. C. (1979). Observation of magnetic flux ropes in the Venus ionosphere. *Nature*, *279*(5714), 616–618. https://doi.org/10.1038/279616a0

Schwartz, S. J. (1998). Shock and discontinuity normals, Mach numbers, and related parameters. In *ISSI Scientific Reports Series*, (Vol. 1, pp. 249–270). Netherlands: ISSI/ESA, Noordwijk.

Schwartz, S. J., Chaloner, C. P., Christiansen, P. J., Coates, A. J., Hall, D. S., Johnstone, A. D., et al. (1985). An active current sheet in the solar wind. *Nature*, *318*(6043), 269–271. https://doi.org/10.1038/318269a0

Schwartz, S. J., Paschmann, G., Sckopke, N., Bauer, T. M., Dunlop, M., Fazakerley, A. N., & Thomsen, M. F. (2000). Conditions for the formation of hot flow anomalies at Earth's bow shock. *Journal of Geophysical Research*, *105*(A6), 12,639–12,650. https://doi.org/10.1029/1999JA000320

Shen, C., Li, X., Dunlop, M., Shi, Q. Q., Liu, Z. X., Lucek, E., & Chen, Z. Q. (2007). Magnetic field rotation analysis and the applications. *Journal of Geophysical Research: Space Physics*, *112*(A6), A06211. https://doi.org/10.1029/2005JA011584

Shi, Q. Q., Shen, C., Pu, Z. Y., Dunlop, M. W., Zong, Q.-G., Zhang, H., et al. (2005). Dimensional analysis of observed structures using multipoint magnetic field measurements: Application to cluster. *Geophysical Research Letters*, *32*(12), L12105. https://doi.org/10.1029/2005GL022454

Shi, Q. Q., Tian, A. M., Bai, S. C., Hasegawa, H., Degeling, A. W., Pu, Z. Y., et al. (2019). Dimensionality, coordinate system and reference frame for analysis of in-situ space plasma and field data. *Space Sci. Rev*, *215*(4), 1, 35–54. https://doi.org/10.1007/s11214-019-0601-2

Sibeck, D. G. (1990). A model for the transient magnetospheric response to sudden solar wind dynamic pressure variations. *Journal of Geophysical Research*, *95*(A4), 3755–3771. https://doi.org/10.1029/JA095iA04p03755

Slavin, J. A., & Holzer, R. E. (1981). Solar wind flow about the terrestrial planets. I - Modeling bow shock position and shape. *Journal of Geophysical Research*, *86*(11), 401–11,418. https://doi.org/10.1029/JA086iA13p11401

Slavin, J. A., Lepping, R. P., Gjerloev, J., Fairfield, D. H., Hesse, M., Owen, C. J., et al. (2003). Geotail observations of magnetic flux ropes in the plasma sheet. *Journal of Geophysical Research: Space Physics*, *108*(A1), SMP 10–11-SMP 10–18. https://doi.org/10.1029/2002JA009557

Smith, C. W., L'Heureux, J., Ness, N. F., Acuña, M. H., Burlaga, L. F., & Scheifele, J. (1998). The ACE magnetic fields experiment. *Space Sci. Rev.*, *86*, 613–632. https://doi.org/10.1023/A:1005092216668

Sonnerup, B. U. Ö., & Cahill, L. J. (1967). Magnetopause structure and attitude from explorer 12 observations. *Journal of Geophysical Research*, *72*(1), 171. https://doi.org/10.1029/jz072i001p00171

Sonnerup, B. U. Ö., Papamastorakis, I., Paschmann, G., & Lühr, H. (1987). Magnetopause properties from AMPTE/IRM observations of the convection electric field: Method development. *J. Geophys. Res*, *92*(A11), 12,137–12,159. https://doi.org/10.1029/JA092iA11p12137

Sun, W. J., Slavin, J. A., Tian, A. M., Bai, S. C., Poh, G. K., Akhavan-Tafti, M., et al. (2019). MMS study of the structure of ion-scale flux ropes in the Earth's cross-tail current sheet. *Geophysical Research Letters*, *46*(12), 6168–6177. https://doi.org/10.1029/2019GL083301

Thomsen, M. F., Gosling, J. T., Bame, S. J., Quest, K. B., Russell, C. T., & Fuselier, S. A. (1988). On the origin of hot diamagnetic cavities near the Earth's bow shock. *Journal of Geophysical Research*, *93*(A10), 11,311–11,325. https://doi.org/10.1029/JA093iA10p11311

Thomsen, M. F., Thomas, V. A., Winske, D., Gosling, J. T., Farris, M. H., & Russell, C. T. (1993). Observational test of hot flow anomaly formation by the interaction of a magnetic discontinuity with the bow shock. *Journal of Geophysical Research*, *98*(A9), 15,319–15,330. https://doi.org/10.1029/93JA00792

Turner, D. L., Wilson, L. B., Liu, T. Z., Cohen, I. J., Schwartz, S. J., Osmane, A., & Burch, J. L. (2018). Autogenous and efficient acceleration of energetic ions upstream of Earth's bow shock. *Nature*, *561*(7722), 206–210. https://doi.org/10.1038/s41586-018-0472-9

Wang, S., Chen, L.-J., Bessho, N., Hesse, M., Wilson, L. B., Giles, B., et al. (2019). Observational evidence of magnetic reconnection in the terrestrial bow shock transition region. *Geophysical Research Letters*, *46*(2), 562–570. https://doi.org/10.1029/2018GL080944

Wang, S., Zong, Q.-G., & Zhang, H. (2013a). Cluster observations of hot flow anomalies with large flow deflections: 1. Velocity deflections. *Journal of Geophysical Research*, *118*, 732–743. https://doi.org/10.1002/jgra.50100

Wang, S., Zong, Q.-G., & Zhang, H. (2013b). Cluster observations of hot flow anomalies with large flow deflections: 2. Bow shock geometry at HFA edges. *Journal of Geophysical Research*, *118*, 418–433. https://doi.org/10.1029/2012JA018204

Wang, S., Zong, Q.-G., & Zhang, H. (2013c). Hot flow anomaly formation and evolution: Cluster observations. *Journal of Geophysical Research*, *118*, 4360–4380. https://doi.org/10.1002/jgra.50424

Wilson, L. B. III, Sibeck, D. G., Turner, D. L., Osmane, A., Caprioli, D., & Angelopoulos, V. (2016). Relativistic electrons produced by foreshock disturbances observed upstream of Earth's bow shock. *Physical Review Letters*, *117*(21), 215,101. https://doi.org/10.1103/PhysRevLett.117.215101

Zhang, H., Sibeck, D. G., Zong, Q. G., Gary, S. P., McFadden, J. P., Larson, D., et al. (2010). Time history of events and macroscale interactions during substorms observations of a series of hot flow anomaly events. *Journal of Geophysical Research*, *115*(A12), A12235. https://doi.org/10.1029/2009JA015180

Zhao, L. L., Zhang, H., & Zong, Q. G. (2017). A statistical study on hot flow anomaly current sheets, J. Geophys. Res. *Space Physics*, *122*(1), 235–248. https://doi.org/10.1002/2016JA023319

Zhao, L. L., Zong, Q.-G., Zhang, H., & Wang, S. (2015). Case and statistical study on evolution of hot flow anomalies. *Journal of Geophysical Research: Space Physics*, *120*(8), 6332–6346. https://doi.org/10.1002/2014JA020862

Zong, Q.-G., et al. (2004). Cluster observations of earthward flowing plasmoid in the tail. *Geophysical Research Letters*, *31*(18), L18803. https://doi.org/10.1029/2004GL020692